

AD

TECHNICAL REPORT ARCCB-TR-00015

**CANNON COATING EROSION MODEL
WITH UPDATED M829E3 EXAMPLE**

SAMUEL SOPOK

OCTOBER 2000



**US ARMY ARMAMENT RESEARCH,
DEVELOPMENT AND ENGINEERING CENTER
CLOSE COMBAT ARMAMENTS CENTER
BENÉT LABORATORIES
WATERVLIET, N.Y. 12189-4050**



APPROVED FOR PUBLIC RELEASE; DISTRIBUTION UNLIMITED

DMIC QUALITY INSPECTED 4

20001115 063

DISCLAIMER

The findings in this report are not to be construed as an official Department of the Army position unless so designated by other authorized documents.

The use of trade name(s) and/or manufacturer(s) does not constitute an official endorsement or approval.

DESTRUCTION NOTICE

For classified documents, follow the procedures in DoD 5200.22-M, Industrial Security Manual, Section II-19, or DoD 5200.1-R, Information Security Program Regulation, Chapter IX.

For unclassified, limited documents, destroy by any method that will prevent disclosure of contents or reconstruction of the document.

For unclassified, unlimited documents, destroy when the report is no longer needed. Do not return it to the originator.

REPORT DOCUMENTATION PAGE			Form Approved OMB No. 0704-0188	
Public reporting burden for this collection of information is estimated to average 1 hour per response, including the time for reviewing instructions, searching existing data sources, gathering and maintaining the data needed, and completing and reviewing the collection of information. Send comments regarding this burden estimate or any other aspect of this collection of information, including suggestions for reducing this burden, to Washington Headquarters Services, Directorate for Information Operations and Reports, 1215 Jefferson Davis Highway, Suite 1204, Arlington, VA 22202-4302, and to the Office of Management and Budget, Paperwork Reduction Project (0704-0188), Washington, DC 20503.				
1. AGENCY USE ONLY (Leave blank)		2. REPORT DATE October 2000		3. REPORT TYPE AND DATES COVERED Final
4. TITLE AND SUBTITLE CANNON COATING EROSION MODEL WITH UPDATED M829E3 EXAMPLE			5. FUNDING NUMBERS PRON No. GENERAL DYNAMICS	
6. AUTHOR(S) Samuel Sopok				
7. PERFORMING ORGANIZATION NAME(S) AND ADDRESS(ES) U.S. Army ARDEC Benet Laboratories, AMSTA-AR-CCB-O Watervliet, NY 12189-4050			8. PERFORMING ORGANIZATION REPORT NUMBER ARCCB-TR-00015	
9. SPONSORING / MONITORING AGENCY NAME(S) AND ADDRESS(ES) U.S. Army ARDEC Close Combat Armaments Center Picatinny Arsenal, NJ 07806-5000			10. SPONSORING / MONITORING AGENCY REPORT NUMBER	
11. SUPPLEMENTARY NOTES Presented at the 36 th AIAA Joint Propulsion Conference, Huntsville, AL, 16-19 July 2000. Published in proceedings of the conference.				
12a. DISTRIBUTION / AVAILABILITY STATEMENT Approved for public release; distribution unlimited.			12b. DISTRIBUTION CODE	
13. ABSTRACT (Maximum 200 words) Cannons with bore coatings are necessary to reduce erosion in current and future high-performance combat systems. In 1996, we developed a unique erosion model for cannons with bore coatings. Since that time, our results from this model have been published for a number of important Army and Navy gun systems with bore coatings. The erosion model for cannons with bore coatings is guided and calibrated and correlates very well with considerable gun system firing data and subsequent laboratory analysis of fired specimens. Our confidence in the model has grown yearly such that we have decided to publish the details of this model. Coated cannon bore erosion does not simply proceed in an outward to inward progressive ablative fashion, since coatings typically spall instead of progressively ablate. This is the only known erosion model for cannons with bore coatings to account for all aspects of the typical firing-induced cannon erosion mechanism. The typical mechanism includes: <ul style="list-style-type: none"> • Heat-check cracking of the bore coating • Bore coating shrinkage leading to progressive widening of these cracks • Combustion gas-induced interface degradation of the exposed substrate metal • Abrupt interfacial spalling of the bore coating platelets due to linked interfacial degradation that forms pits • Subsequent substrate metal gas wash-to-erosion condemnation A very fine bore coating crack provides a narrow combustion gas path to the metal substrate thus producing limited interfacial substrate degradation. In contrast, a progressively widened/extended bore coating crack due to firing-induced bore coating shrinkage provides a wide combustion gas path to the metal substrate producing substantial interfacial substrate degradation. The purpose of this report is to review typical cannon erosion mechanisms, highlight the resultant cannon coating erosion model, show how this very critical coatings model incorporates into our overall cannon erosion code, and provide an example. The example is an updated erosion prediction for the experimental nonablative M829E3 kinetic energy tank round with and without HEAT-type rounds. The presence of HEAT-type rounds significantly alters the M829E3 erosion pattern compared to their absence.				
14. SUBJECT TERMS Cannon Coatings, Erosion Modeling, M829E3 Erosion Simulation			15. NUMBER OF PAGES 22	
			16. PRICE CODE	
17. SECURITY CLASSIFICATION OF REPORT UNCLASSIFIED	18. SECURITY CLASSIFICATION OF THIS PAGE UNCLASSIFIED	19. SECURITY CLASSIFICATION OF ABSTRACT UNCLASSIFIED	20. LIMITATION OF ABSTRACT UL	

TABLE OF CONTENTS

	<u>Page</u>
INTRODUCTION.....	1
COMPUTATIONAL AND EXPERIMENTAL METHODS.....	1
RESULTS AND DISCUSSION	2
REFERENCES.....	12

LIST OF ILLUSTRATIONS

1. M829E3 NOVA gas pressure.....	13
2. M829E3 NOVA gas temperature.....	13
3. M829E3 MABL recovery enthalpy.....	14
4. M829E3 MABL cold wall heat flux	14
5. M829E3 CCET gas/wall thermochemistry	15
6. M829E3 M256 substrate exposure.....	15
7. M829E3 peak enabling erosion step	16
8. M829E3 peak accelerating erosion step.....	16
9. M829E3 HC chromium surface temperature	17
10. M829E3 MACE A723 interface temperature	17
11. M829E3 MACE A723 surface temperature.....	18
12. M829E3 exposed interface temperature.....	18
13. M829E3 erosion onset.....	19
14. M829E3 erosion condemnation	19
15. M829E3 erosion summary	20
16. E3/HEAT M256 substrate exposure	20
17. M829E3/HEAT erosion summary	21

INTRODUCTION

Our initial rocket-derived model that was introduced in 1995 was quite successful for predicting erosion on uncoated and nitrided steel cannon bores (ref 1). For coated steel cannon bores, all other known bore erosion models, including our initial rocket-derived model, incorrectly ignore or progressively ablate the bore coating before progressively ablating the metal substrate (ref 1). By ignoring or progressively ablating the bore coating, these models do not correctly address the above heat-checking, crack widening, interface degradation, or abrupt coating platelet spalling of the bore coating. Our practical thermal-chemical-mechanical erosion model for cannons with bore coatings is derived and developed from very successful ballistic missile and space program reentry vehicle codes that evaluated nose-tips, heat shields, and nozzles. This cannon erosion model consists of a number of linked thermochemistry, interior ballistic, boundary layer, thermal, erosion, and bore coating codes. These codes are used to predict wall temperature profiles and erosion profiles in coated cannon bores as a function of position, time, and round history. Pressure gauge, radar, thermocouple, and kinetic rate data are used to calibrate these codes. The codes receive important inputs for nondestructive and laboratory microscopic materials/chemical analyses of fired specimens. The analyses focus on substrate exposure, coating loss, cracks, pits, interfaces, voids, and surfaces, including their crack/pit frequency, crack/pit width, coating platelet width, wall layers, residues, reactions, diffused species, and phase changes all as a function of position, time, and round history. An improved cannon coating erosion model based on typical refractory metal-coated cannon bore erosion mechanisms (refs 1,2) is given with an unclassified illustrative example of the experimental M829E3 gun system.

COMPUTATIONAL AND EXPERIMENTAL METHODS

Our cannon erosion code consists of a number of interactively linked codes and is used to predict wall temperature profiles and thermal-chemical-mechanical erosion profiles in cannons (refs 1,2). This overall erosion code includes the following:

- Standard nonideal gas/wall thermochemical rocket code modified for guns (CCET) (refs 1-3)
- Standard interior ballistics gun code (XNOVAKTC) (refs 1,2,4)
- Standard heat transfer modified by mass addition to boundary layer rocket code modified for guns (MABL) (refs 1,2,5)
- Standard wall material ablation conduction erosion rocket code modified for guns (MACE) (refs 1,2,6)

The above erosion predictions are guided and calibrated by substantial gun system firing data and fired specimen analyses.

The previous M829E3 modeling effort (ref 2) used 19 pounds of RPD-380 propellant and a classified projectile F-slug weight. The RPD-380 propellant fracturing was not allowed at -32°C despite its glass transition at -29°C, both with/without one pound of ablative paste on a moving projectile base donut. Ablative paste products were not allowed on the bore wall if present. The current M829E3 modeling effort uses 18 pounds of RPD-380 propellant and a 0.3-pound lighter classified projectile F-slug weight. The RPD-380 propellant fracturing is allowed at -32°C due to its glass transition at -29°C, and no ablative paste. A companion paper to this M829E3 modeling effort to be published shortly also uses 18 pounds of RPD-380 propellant and a 0.3-pound lighter classified projectile F-slug weight. In this companion case, the RPD-380 propellant fracturing is allowed at -32°C due to its glass transition at -29°C, and 0.5-pound of ablative paste is used on the combustible case shoulder. Ablative paste products are allowed on the bore wall.

RESULTS AND DISCUSSION

The experimental nonablative M829E3 kinetic energy tank round example with and without significant HEAT-type rounds is used to show the step-by-step process of how the coated cannon erosion model is incorporated into the overall cannon erosion code.

The CCET thermochemistry cannon code uses initial chemical/materials input to calculate gas and thermochemistry data for the interior ballistics, boundary layer, and thermal and erosion codes. The example M829E3/RPD-380 propellant consists of approximately 59% nitrocellulose, 25% nitroglycerine, 15% diethylene glycol dinitrate, and 1% other minor species. Its igniter consists of 25 grams black powder and 25 grams CBI. Actual measured thermochemical data are used to calibrate the calculation for gas products.

The XNOVAKTC interior ballistics code uses thermochemistry code output and gun system defining inputs to calculate the time-dependent core flow data for the boundary layer code. The example gun system includes the 17.3-foot, 120-mm M256 cannon, its experimental nonablative 18-pound RPD-380 propellant, and classified projectile details. Actual measured pressure gauge and muzzle velocity data are used to calibrate this time-dependent core flow calculation.

Figures 1 and 2 show the experimental nonablative M829E3 round XNOVAKTC interior ballistic results for respective maximum values of gas pressure (P_g) and gas temperature (T_g) as a function of selected axial positions at selected round-conditioning temperatures. Maximum values were used instead of time-dependent data to simplify the appearance of these figures. Both decrease with increasing axial position. Gas velocity is omitted due to its classified nature. Selected axial positions included 0.6, 1.6, 2.2, 3.3, and 5.1 meters from the rear face of the tube (RFT), while the selected round-conditioning included the hot (49°C), ambient (21°C), and cold (-31°C) temperatures. These five selected axial positions and three selected round-conditioning temperatures were used exclusively throughout the rest of this report. The significance of the 0.6-meter position is that it is slightly past the origin of the bore, and it is the mean peak eroded position when both M829E3 and HEAT-type rounds are mixed. The significance of the 1.6-meter position is that it is the mean peak eroded position when M829E3 rounds are fired without HEAT-type rounds. The significance of the 2.2-meter position is that it is the mean peak eroded

position when M829A2 rounds are fired without HEAT-type rounds. The significance of the 3.3-meter position is that it is near the bore evacuator holes. The significance of the 5.1-meter position is that it is near the muzzle. Distributions and associated standard deviations exist around these various mean eroded positions.

The MABL boundary layer cannon code uses thermochemistry and interior ballistics code outputs to calculate boundary layer characteristics for the thermal and erosion code. Figures 3 and 4 show the experimental nonablative M829E3 round MABL boundary layer results for respective maximum values of recovery enthalpy (H_r) and cold wall heat flux (Q_{cw}) as a function of selected axial positions at selected round-conditioning temperatures. Maximum values were again used instead of time-dependent data to simplify the appearance of these figures. Both increase with increasing axial position to a 1.6-meter from RFT peak and decrease thereafter to the muzzle. The 0.6-meter from RFT mean peak heat transfer bore position calculated by the interior ballistic analysis is shifted to a 1.6-meter from RFT mean peak bore position calculated by the boundary layer analysis. This is due to the 1600°K combustion case gas cooling effects and turbulent gas mixing/heating effects.

The CCET thermochemistry cannon code uses initial chemical/materials input to calculate gas/wall thermochemistry data for the thermal and erosion code. Actual measured thermochemical data are used to calibrate the calculation for gas/wall products and gas/wall reaction rates. Figure 5 shows the experimental nonablative M829E3 round CCET thermochemical results for mean values of reacting gas/wall enthalpy (H_{gw}) and thermochemical ablation potential (B_a) as a function of wall temperatures (T_{wall}) for the high contraction (HC) chromium plate/gun steel substrate wall materials. Mean values were used to simplify the appearance of this figure.

The MACE thermal and erosion cannon code uses thermochemistry code output, boundary layer code output, material properties input, and firing history/scenario input to calculate wall temperature profiles and thermal-chemical-mechanical wall erosion profiles as a function of axial position, radial position, time, and firing history/scenario. The following data types are used to calibrate this wall thermal and erosion calculation:

- Actual measured gas/wall kinetic rate function input data
- Measured thermocouple input data
- Measured destructive/nondestructive microscopic coating and steel loss/void input data (cracks, pits, interfaces, surfaces)
- Measured destructive reaction/diffusion/phase change degradation layer input data (cracks, pits, interfaces, surfaces)

The measurement and use of these four types of data are explained in the remainder of the report.

Measured gas/wall kinetic rate function data are used to calibrate the thermochemical calculation and transform this chemical equilibrium calculation into a partial chemical kinetic calculation. Chemical analysis of crack and pit wall layers, interface wall layers, bore surface layers, subsurface void residues, and surface residues further guide gas/wall kinetics calibration. Thermocouple data are used to calibrate the wall thermal profile calculation.

Figure 6 shows typical gun steel substrate exposure for cannons with a mixture of experimental nonablatives M829E3 rounds and other kinetic energy rounds. These data are from a small sampling of HC chromium plated M256 cannons that quantify cracking, pitting, and chromium plate loss. These cannons were condemned due to erosion and had numerous condemned scoring holes centered at the 1.6-meter from RFT position. The substrate exposure is a function of the selected axial positions at 1% (nondestructively measured at post-proofing), 50% (exponentially estimated), 80% (exponentially estimated), and 100% (nondestructively and destructively measured at erosion condemnation) of equivalent ambient-conditioned M829E3 erosion life based on previous work (ref 2).

The nondestructive substrate exposure measurements are taken by a magnifying borescope with a calibrated scale, while metallographic, SEM-EDS, and ESCA techniques take the corresponding destructive measurements. These nondestructive measurements are based on the verified assumption that substrate exposure is approximately equal at the surface and interface. Bore position-dependent and equivalent erosion life-dependent substrate exposure measurements include average axial and circumferential crack/pit frequency, average axial and circumferential crack/pit width, and average axial and circumferential platelet width. An improved comprehensive measurement procedure is often used that includes crack/pit frequency, crack/pit width, and platelet width distributions instead of simple averaging. These measured data are used as a substitute for a thermal-mechanical crack and pit model that is yet to be developed. The measured substrate exposure pattern correlates with the boundary layer heat-transfer pattern where both increase with increasing axial position to a 1.6-meter from RFT peak and decrease thereafter to the muzzle.

Figure 7 (2000x) and Figure 8 (1000x) are micrographic examples of destructive substrate exposure measurements taken by an SEM-EDS technique, but metallographic, EPMA, and ESCA techniques also gave similar micrographic results. For the M829E3 1.6-meter from RFT peak eroded position, these figures respectively illustrate very typical enabling and accelerating erosion mechanism steps. Figure 7 shows a very fine HC chromium plate crack that provides a narrow combustion gas path to the gun steel, thus producing limited interfacial gun steel degradation. In contrast, Figure 8 shows a progressively widened/extended HC chromium plate crack caused by chromium shrinkage that provides a wide combustion gas path to the gun steel producing substantial interfacial gun steel degradation. If this cannon were still in service, linked interfacial degradation of the main crack to the adjacent fine crack in Figure 8 would lead to eventual spalling of the associated chromium platelet. All three cracks in these two figures are completely through the chromium plate coating. Thermally induced crack widening due to chromium shrinkage is not a valued bore coating property. For the HC chromium coating alloy, thermally induced chromium shrinkage results in yielding, observed/measured nonmetallic out-gassing, and observed restructuring to a more organized and compact state. Using the above techniques

coupled with their associated chemical analysis techniques, these and similar micrographs illustrate phase change degradation (diffusion-induced carburized white layer and heat-affected zone on/into exposed gun steel, chromium recrystallization), and chemical reaction degradation (oxidation and sulfidation of exposed gun steel forming semi-metallic layers) of the gun steel substrate under the 130 μm thick chromium plate and particularly at crack and interfacial walls/wall layers.

Two other factors that enhance chromium plate/gun steel substrate interfacial degradation of its metals and interstitials are the increased reactivity of the interface due to its higher energy state and interfacial porosity due to firing-induced local diffusion (ref 1). For refractory metal coated steels, a group from LSU has found that surface refractory metal coating oxides seed heat-checking cracks, high temperature combustion oxidizes steel crack walls and interfaces forming brittle products with inferior mechanical properties, and atomic hydrogen hops between crack wall oxides to migrate to its lowest free energy at a crack tip (ref 7).

The HC chromium plate has a passivating oxidation temperature at about 2000°K, a sulfidation temperature above 2130°K, and a melting point at about 2130°K. Gun steel has an expansive flaking iron oxidation temperature at about 1050°K, an iron sulfidation temperature at about 1270°K, an iron oxide melting point at about 1640°K, an iron sulfide melting point at about 1470°K, and a gun steel melting point at about 1720°K.

Figures 9 through 11 show the respective experimental nonablative M829E3 MACE maximum wall temperature (T_{wall}) results for the HC chromium surface, gun steel interface, and gun steel surface minus 0.13-mm as a function of the selected axial positions at the selected round-conditioning temperatures. For these figures, maximum values were also used instead of time-dependent data to simplify their appearance. The maximum wall temperature for the HC chromium surface is about 1700°K, which explains its inertness. The maximum wall temperature for the unexposed nonreacting gun steel interface is about 1270°K, which explains its reactivity. The maximum wall temperature for the fully exposed reacting gun steel surface (0.13-mm below bore surface due to HC chromium spalling) is about 1440°K, which explains its reactivity. The maximum wall temperature for this same nonreacting gun steel surface is about 1775°K. For these three figures, the calculated maximum wall temperature patterns correlate with the boundary layer heat-transfer pattern, where both increase with increasing axial position to a 1.6-meter from RFT peak and decrease thereafter to the muzzle.

The following thermal data illustrate the relationship between tank, artillery, and medium caliber gun systems. Advanced M256 kinetic energy rounds produce ~1.5 (100k/65k) times the peak pressure, ~1.0 (3300/3300) times the velocity at peak pressure, and ~1.0 (3450/3550) times the peak temperature of advanced M242 kinetic energy rounds. The M256 round results in ~1.5 times the peak heat transfer rate, and also ~1.5 times the peak film coefficient of the M242 round. Advanced XM297 zone six rounds produce ~0.6 (60k/100k) times the peak pressure, ~0.7 (2150/3300) times the velocity at peak pressure, and ~0.9 (3000/3450) times the peak temperature of advanced M256 kinetic energy rounds. The XM297 round results in ~0.4 times the peak heat transfer rate and ~0.4 times the peak film coefficient of the M256 round (ref 8). Although there is a similarity between the heat-transfer rate and the film coefficient in a given

gun system, the peak heat transfer rate varies significantly from these large caliber gun systems to their medium caliber counterparts.

Now that the typical erosion mechanisms for coated cannons have been reviewed, it will be shown how these mechanisms are modeled and incorporated into our overall cannon erosion code. Core flow gases at the combustion gas temperature collide with the bore surface and convectively transfer a portion of their energy to the wall. This fully convective bore surface heating is related to the bore surface temperature.

When a bore coating platelet spalls and forms a pit that is at least 33% wider than the coating thickness depth, then a portion of the core flow combustion gases collide with the exposed substrate interface and convectively transfer a portion of their energy to the interface at a rate approximately equal to that of the bore surface. The fully convective substrate interface heating is related to that exposed substrate interface temperature and approximately equal to the fully exposed substrate bore surface temperature that is actually 0.13-mm below the original bore surface due to HC chromium spalling. The wide pit-maximum convective heating of the substrate interface is designated case one. The HC chromium coating thickness is typically 0.005 inch, and the minimum required pit width for fully convective heating is about 0.0067 inch for the experimental M829E3 round.

When a bore coating platelet spalls forming a pit that is progressively narrower than case one's pit width, then a progressively decreasing portion of the core flow combustion gases collide with the partially exposed substrate interface. This results in the convective transfer of a portion of the energy to this partially exposed interface at a rate that is progressively less than that of the fully exposed substrate bore surface due to the increase of energy-reducing collisions. The progressively decreasing convective substrate interface heating is related to that partially exposed substrate interface temperature and progressively less than the above exposed gun steel bore surface temperature. As the crack/pit width progressively narrows, the mean free path of the gas molecules decreases due to energy-reducing collisions prior to the interface that reduce the convective heat transfer rate to a value that is progressively closer to that of the unexposed conductive heat transfer rate of the interface. The transition from wide to infinitesimally small crack/pit-transition from maximum to infinitesimally small convective heating of the substrate interface is designated case two.

When a bore coating has a very fine crack forming an infinitesimally narrow pit, then the core flow combustion gases never reach the substrate interface without many energy-reducing collisions that reduce the convective heat transfer rate to that of the unexposed substrate interface conductive heat transfer rate. The infinitesimally small convective substrate interface heating is related to that interface temperature and approximately equals the fully conductive unexposed substrate interface temperature. This model includes initial high-pressure filling of cracks and pits. The infinitesimally small crack/pit with infinitesimally small convective heating of the substrate interface is designated case three. Very fine HC chromium crack widths are typically 0.00005 inch for the experimental M829E3 round.

A cubic function of the general form $y = a + bx^3$ uses the above fully convective heating case one and fully conductive heating case three extremes for calibration to predict a resultant substrate interface temperature for a given crack/pit width as follows:

$$T_{iy} = T_{iu} + [((T_s - T_{iu})/W_c^3)(W_x^3)] \quad (1)$$

where

- T_{iy} is the resultant calculated substrate interface temperature for a given crack/pit width.
- T_{iu} is the calculated fully conductive/unexposed substrate interface temperature of a very small crack/pit width, which is approximately equal to the fully conductive/unexposed substrate interface temperature from Figure 10.
- T_s is the calculated fully convective/exposed substrate surface temperature for crack/pit width that is at least 33% greater than the coating thickness depth, which is approximately equal to the fully exposed reacting substrate surface temperature from Figure 11 (substrate surface is 0.13-mm below the bore surface due to HC chromium spalling).
- W_c is the measured fully convective/exposed crack/pit width that is at least 33% greater than the coating thickness depth from micrographs similar to Figures 7 and 8.
- W_x is a measured given crack/pit width from substrate exposure data that generated Figure 6.

The first term on the right is the y-intercept that is the substrate interface temperature due to conductive heating. The second term on the right in brackets is the associated temperature correction for convective heating that ranges from infinitesimally small to the difference between $T_s - T_{iu}$. The T_{iy} value changes slowly at first with increasing W_x and then more rapidly as it approaches W_c due to the cubic function. For similar cracks/pits, T_{iy} in this equation varies significantly with axial position, time, and rounds history. Exposed substrate interface temperatures are calculated for the life of each crack and pit. For a gun system that has not been built or fired, crack/pit data can possibly be approximated from a similar gun system. Using this equation, Figure 12 shows the calibrating extreme measured points and the calculated interior points for the nonablative M829E3 maximum exposed interface temperature as a function of HC chromium crack/pit width at selected axial positions and 49°C round conditioning.

An exponential fit was also used and gave very similar results compared to this cubic function. Since the meaning of the coefficients for the cubic function was easier to determine compared to that of the exponential function, we opted to use the better-understood cubic fit given in equation (1). For the cubic fit in equation (1), it is important to note that its "constant" coefficients are not really constant and vary by axial position, time, rounds history, and gun system.

Equation (1) correlates and has been successfully applied to numerous advanced medium and large caliber gun systems over the last four years, based on measured firing-related data from their most extreme rounds. The measurements include phase change degradation data (diffusion-

induced carburized white layer and heat-affected zone on/into exposed gun steel, chromium recrystallization) and chemical reaction degradation data (oxidation and sulfidation of exposed gun steel forming semi-metallic layers). The existence and depth of these measured degradations into the exposed gun steel substrate depends on and correlates with the magnitude of the related positional-dependent wall temperature profiles. These measurements were particularly focused on the exposed gun steel substrate at the crack/pit/interface walls and wall layers.

After the resultant substrate interface temperatures in cracks/pits are calculated for the position, time, and round-dependent crack/pit widths, then the heat transfer multipliers in the MACE code are adjusted on a trial and error basis to achieve the resultant substrate interface temperatures and their corresponding substrate interface ablation rates. The adjustment of these heat transfer multipliers raises the associated T_{iu} values to the resultant T_{iy} values. Surface ablation rates are calculated directly by the MACE code and do not require a previous calculation using equation (1). In addition, as the measurable interface degradation progresses, the interface contact variable in the MACE code is adjusted as a function of axial position and rounds history as the measurable interface degradation progresses. The transition from fully-conductive to fully-convective substrate interface temperature extremes is computed for the erosion life of each crack and pit based on position, time, and round-dependent substrate exposure data. Exposed substrate interface ablation rates are calculated for the life of each crack and pit.

Steel substrate degradation of interfaces, cracks, pits and surfaces is computed by the area under a temperature-time curve above a degradation threshold such as:

- The 1000°K transformation onset of steel
- The 1050°K oxidation onset of iron by oxygen
- The 1270°K oxidation onset of iron by sulfur
- The 1420°K melting point onset of iron carbide
- The 1470°K melting point onset of the iron-sulfur compound
- The 1640°K melting point onset of the iron-oxygen compound
- The 1720°K melting point onset of gun steel

Calibrated diffusion-controlled transformation codes (THERMOCALC, DICTRA) are used to evaluate multi-component gun steel system transformations.

The exposed steel interface degradation thickness is measurable as a function of position and round history. This exposed steel interface degradation thickness under a chromium platelet is consumed in a linear strand-burning fashion by the associated T_{iy} ablation rate above the ablation threshold. When any type of degradation of the exposed gun steel interface thickness under this coating platelet merges from all adjacent cracks/pits, then the coating platelet spalls and gas wash onset begins.

Heat and diffused species are transferred inward in an exponentially-decaying fashion from exposed steel substrate interface crack/pit walls surrounding an unexposed substrate interface thickness under a coating platelet. Extreme heating and diffusion of the substrate

interface thickness results in transformation, interstitial occupation, and reactions that may merge leading to complete degradation of the interface thickness, subsequent mechanically-assisted bore coating platelet spalling, and substrate gas wash. This transformation of the gun steel substrate to untempered martensite merges inward from all adjacent crack/pit walls leading to complete degradation of the interface and subsequent coating platelet spalling. In a similar fashion but to a lesser extent and lesser-associated distance inward, diffusion species are transferred inward from all adjacent crack/pit walls in an exponentially decaying fashion. These diffused species result in interstitial occupation and/or reactions of the gun steel substrate, thus leading to degradation of the interface and subsequent coating platelet spalling.

Very few type-classified or experimental cannons are spared the eventual heat-checking of their bore coatings. A crack or pit of any kind in the brittle M256 HC chromium coating provides a mass transport path to the gun steel. Severe (wide) or frequent bore coating heat-checking cracks/pits result in respective exponential and linear growth of erosion. Increasing either exposes the gun steel substrate interface to more hot combustion gases. Using nondestructive and laboratory microscopic analyses of fired specimens, it is important to measure how much of the steel substrate is exposed as a function of position, time, and firing history/scenario. Progressively increasing the crack or pit width for a given crack frequency and heating profile results in exponential growth of the exposed substrate interface temperature. This is due to increased convective heating of that interface from increased core flow gas collisions. Progressively increasing the crack or pit frequency (decreasing both the interface and coating platelet widths) for a given crack width and heating profile results in linear growth of the bi-directional percentage of substrate interface degradation under a bore coating platelet due to decreasing the degradation's merging distance.

Additionally, exponential growth of erosion results from progressive temperature increases above each of the mentioned gas/wall reaction thresholds due to exponential growth of combustion gas/exposed substrate interface reactions. Again, using nondestructive and laboratory microscopic materials/chemical analyses of fired specimens, it is important to measure the achievement of and level above these reaction thresholds as a function of position, time, and round history. Based on the Arrhenius equation, the reaction rate above the combustion gas/exposed interfacial substrate wall reaction threshold rises exponentially with increasing temperature. Combustion gas chemistry plays a role in increasing gas/wall reaction rates. This bore coating erosion model requires measurable gas/wall bore coating and steel substrate reactivity data as a function of pressure, temperature, and velocity. When these data are not available in the literature, they are measured in-house for each gun system material/configuration using specialized gas/wall kinetic rate/Arrhenius testers.

Using the coupled MACE and coatings model calculations, Figures 13 and 14 show the experimental nonablative M829E3 round cumulative erosion results. These include the respective values of cumulative rounds to 0.13-mm erosion (gun steel gas wash onset) and 5-mm erosion (erosion condemnation) as a function of the selected axial positions at selected round-conditioning temperatures. The data in these two figures inversely correlate with the predicted M829E3 boundary layer heat transfer and substrate exposure patterns above where the erosion values decreased to a 1.6-meter from RFT minimum and increased thereafter. In Figure 13, the chromium plate loss at the muzzle is due to purely mechanical effects.

Figure 15 is simply a summary of Figures 13 and 14 at only the erosion condemnation governing the 1.6-meter from RFT peak eroded position. Cumulative erosion versus cumulative equivalent M829E3 rounds at 1.6-meters from RFT is plotted. For the respective 49°C, 21°C, -32°C, and equal distribution cases at this position, achievement of the 0.13-mm gun steel gas wash onset depth is at about 40, 65, 60, and 55 rounds. Achievement of the 5-mm erosion condemnation depth is at about 130, 210, 190, and 170 rounds. A preliminary estimate for the experimental nonablatively ambient-conditioned M829E3 round erosion effective full charge (EFC) factor is about three based on its M829A2 counterpart (ref 2).

Figure 16 shows typical gun steel substrate exposure for cannons with a mixture of experimental nonablatively M829E3 rounds, HEAT/HEAT trainer-type rounds, and other kinetic energy-type rounds. These data are from a small sampling of HC chromium plated M256 cannons, and quantify cracking, pitting, and chromium plate loss. The cannons were taken out of service at approximately 50% of their erosion life, with peak erosion and numerous scoring holes centered at the 0.6-meter from RFT position. The substrate exposure is a function of the selected axial positions at 1% (nondestructively measured at post-proofing), 50% (nondestructively and destructively measured at removal from service), 80% (exponentially estimated), and 100% (exponentially estimated) of equivalent ambient-conditioned M829E3 erosion life based on previous work (ref 2).

Figure 16 dramatically differs from Figure 6, which depicts cannons with a mixture of experimental nonablatively M829E3 rounds and other kinetic energy-type rounds. The difference is due to the very noticeable HEAT round fin gouging of the chromed bore surface for the first 0.3-meter of bore travel past the forcing cone, thus producing additional/higher frequency HC chromium cracking/pitting. This additional/higher frequency HC chromium cracking/pitting is not present when HEAT-type rounds are absent. Maximum gouging is centered at the 0.6-meter from RFT position, and diminishes after 0.3-meter of travel down bore. For experimental nonablatively M829E3 rounds, since increased crack/pit frequency (decreased interface width, decreased coating platelet width) linearly increases the rate of erosion, the presence of HEAT round gouging allows erosion to peak at the 0.6-meter from RFT position instead of the normal 1.6-meter from RFT peak eroded position when these HEAT-type rounds are absent. These measurements were taken using techniques similar to Figure 6. For cannons where M829A2, M829A1, or M829 is the most advanced kinetic energy round, measurements have shown that HEAT-type rounds have similarly altered their peak eroded bore positions.

Figure 17 also uses the coupled MACE and coatings model calculations to summarize cumulative erosion results for cannons with a mixture of experimental nonablatively M829E3 rounds, HEAT/HEAT trainer-type rounds, and other kinetic energy-type rounds. These results include the peak eroded 0.6-meter from RFT position as a function of cumulative equivalent M829E3 rounds at the selected round-conditioning temperatures. The peak eroded 0.6-meter from RFT position governs erosion condemnation for this case. For the respective 49°C, 21°C, -32°C, and equal distribution cases at this position, achievement of the 5-mm erosion condemnation depth is at about 120, 200, 180, and 160 rounds. The peak erosion summary results in this figure are similar to the M829E3 peak erosion summary at 1.6 meters from RFT in Figure 15, except that the peaks are centered on two different axial locations.

Erosion mechanisms and their magnitude may vary between/within tank, artillery, and medium caliber gun systems, but our coating erosion model adjusts for these variations. What does cannon erosion correlate with as a function of axial position? Cannon erosion often does not correlate with maximum crack depth, since ablatives and combustible cases unevenly alter erosion patterns and this erosion may unevenly alter (blunt) crack tips as a function of axial position. Cannon erosion often does not correlate with maximum transformation depth, again since ablatives/combustible cases unevenly alter erosion patterns, the heat is used unevenly at the surface/interface, and not all this heat gets into the steel substrate as a function of axial position. Cannon erosion always correlates with maximum interface degradation and substrate exposure. These generalizations hold for tank, artillery, and medium caliber gun cannons.

REFERENCES

1. Dunn, S., Sopok, S., Coats, D., O'Hara, P., Nickerson, G., and Pflegl, G., "Unified Computer Model for Predicting Thermochemical Erosion in Gun Barrels," *Proceedings of 31st AIAA Joint Propulsion Conference*, San Diego, CA, July 1995; Also *AIAA Journal of Propulsion and Power*, Volume 15, Number 4, pp. 601-612.
2. Sopok, S., Loomis, R., Pflegl, G., and Rickard, C., "Preliminary Erosion Analysis for the Experimental M829E3 Kinetic Energy Round," *Proceedings of the 36th JANNAF Combustion Meeting*, NASA Kennedy Space Center, FL, October 1999.
3. Coats, D., Dunn, S., and Sopok, S., "A New Chemical Equilibrium Code with Compressibility Effects," *Proceedings of the 33rd JANNAF Combustion Meeting*, Monterey, CA, October 1996.
4. Gough, P., "The XNOVAKTC Code," Paul Gough Associates, Portsmouth, NH, U.S. Army BRL-CR-627, February 1990.
5. Levine, J., "Transpiration and Film Cooling Boundary Layer Computer Program (MABL) - Numerical Solution of the Turbulent Boundary Layer Equations with Equilibrium Chemistry," NASA Marshall N72-19312, June 1971.
6. Dunn, S., "Materials Ablation Conduction Erosion Program (MACE)," Software and Engineering Associates, Inc., Carson City, NV, June 1989.
7. Kalia, R., "High Temperature Oxidation of Cracks in Refractory Metal Coated Steel," *Proceedings of the American Chemical Society National Meeting*, New Orleans, LA, 1999; also Air Force Research Lab-Kirkland Contractor Report by Department of Physics Concurrent Computing Laboratory for Materials Simulations (CCLMS) at Louisiana State University-Baton Rouge, 1999.
8. Vottis, P., "Heat Transfer in Various Cannon Systems," Private Communication, Benet Laboratories, Watervliet, NY, 2000.

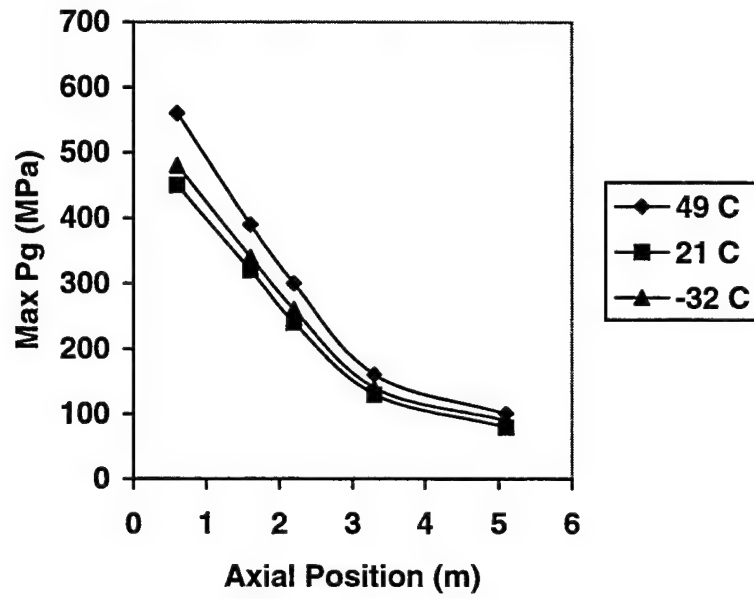


Figure 1. M829E3 NOVA gas pressure.

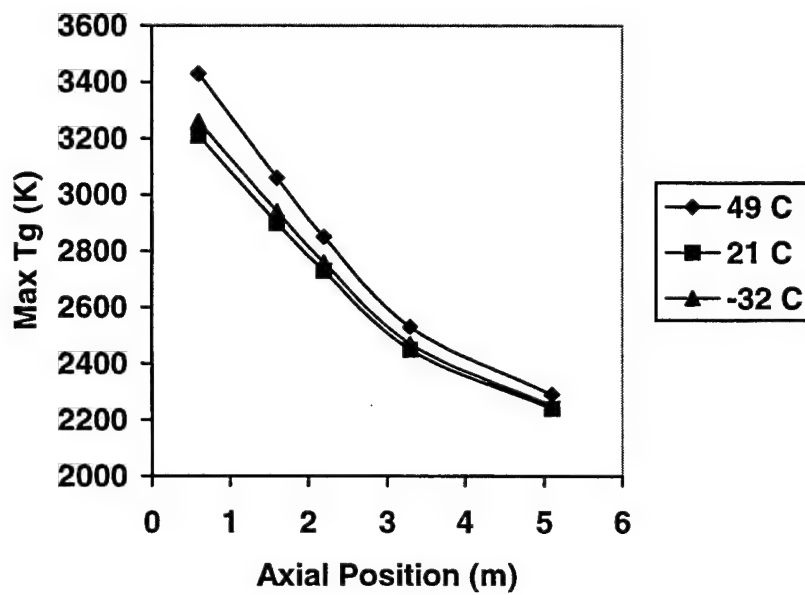


Figure 2. M829E3 NOVA gas temperature.

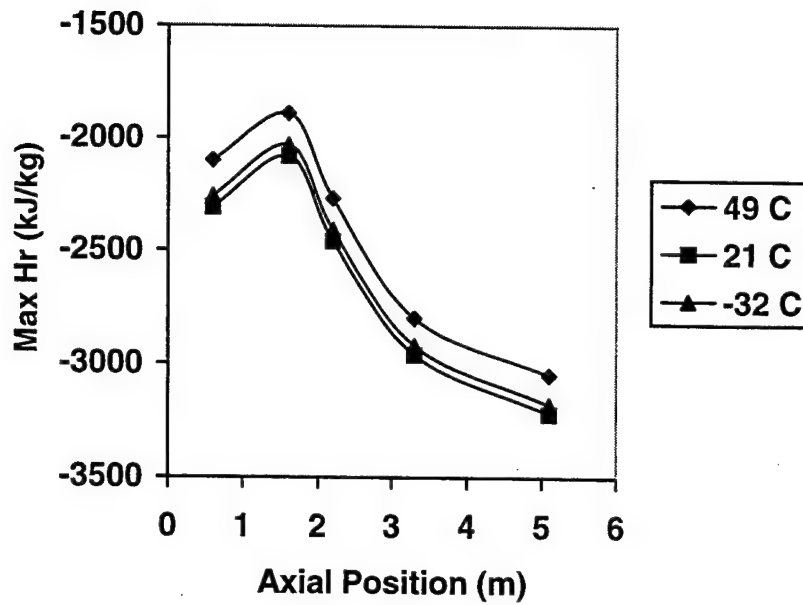


Figure 3. M829E3 MABL recovery enthalpy.

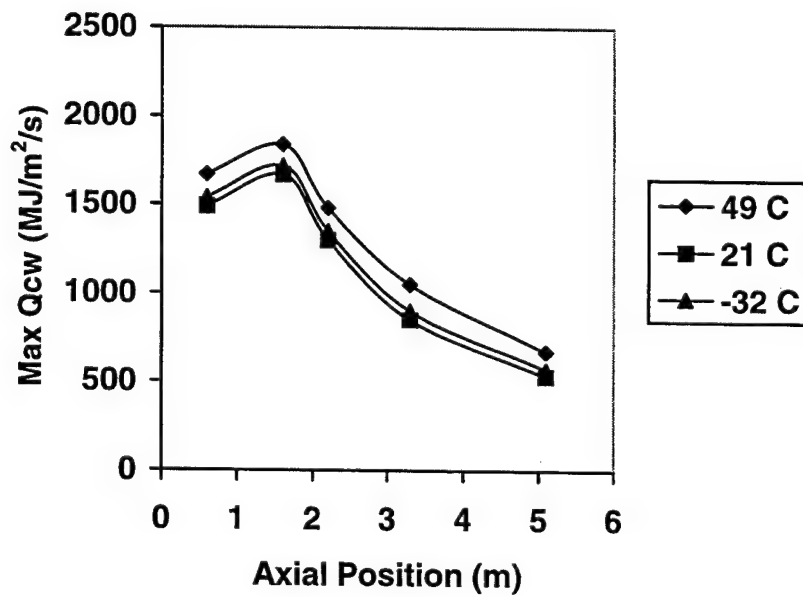


Figure 4. M829E3 MABL cold wall heat flux.

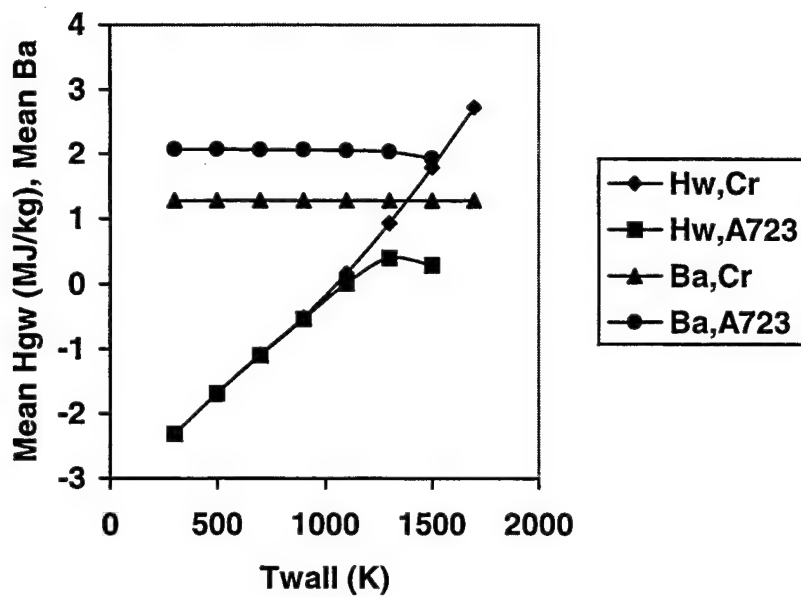


Figure 5. M829E3 CCET gas/wall thermochemistry.

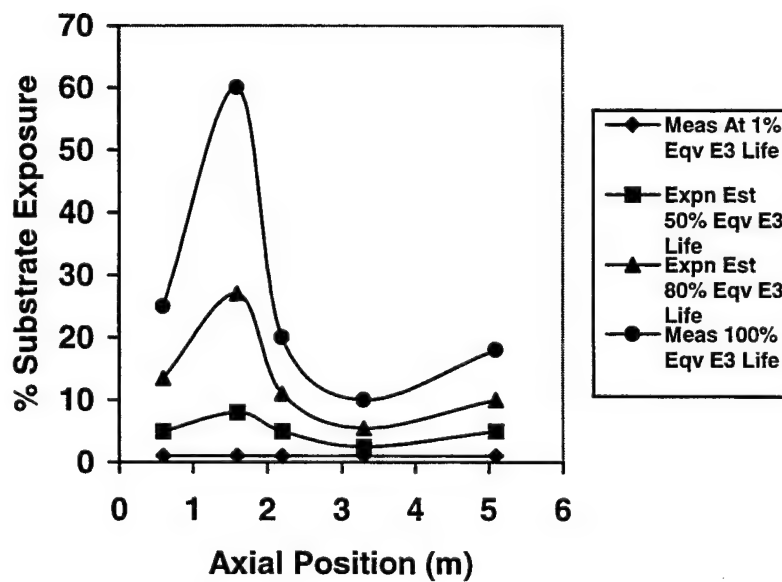


Figure 6. M829E3 M256 substrate exposure.

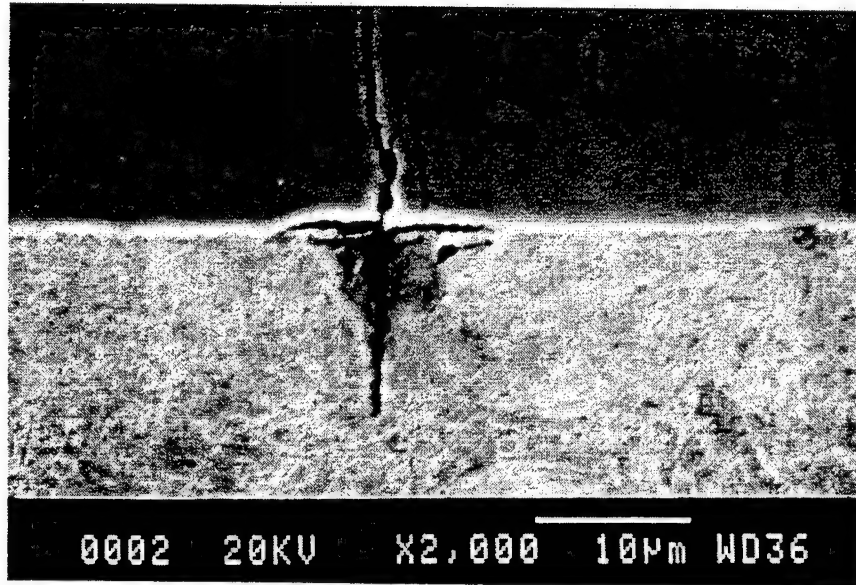


Figure 7. M829E3 peak enabling erosion step.

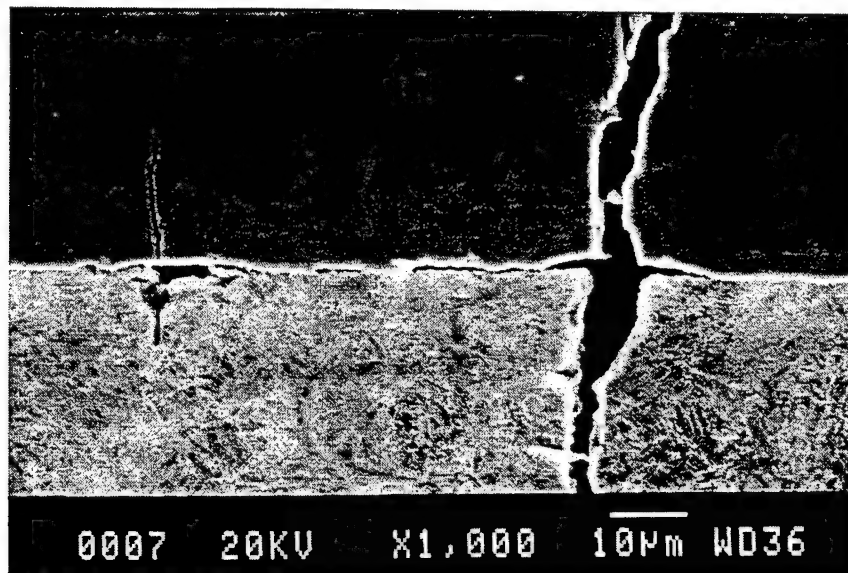


Figure 8. M829E3 peak accelerating erosion step.

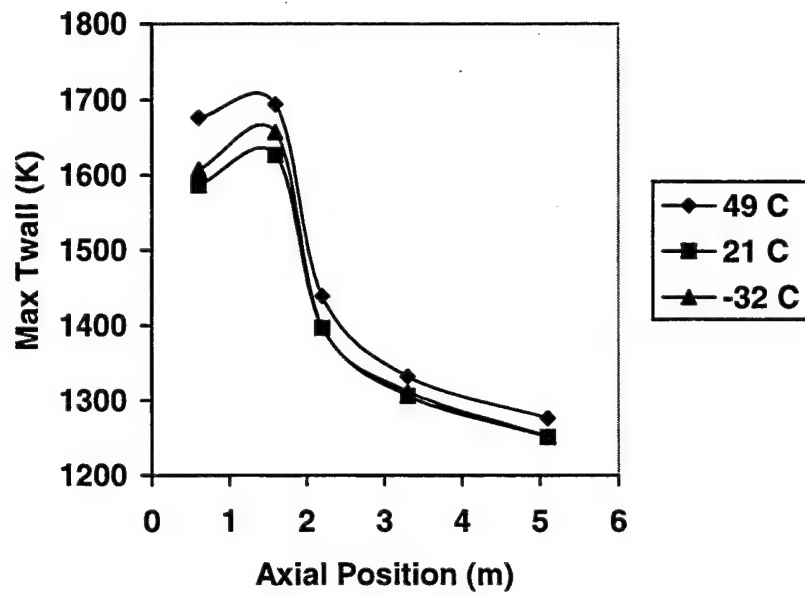


Figure 9. M829E3 HC chromium surface temperature.

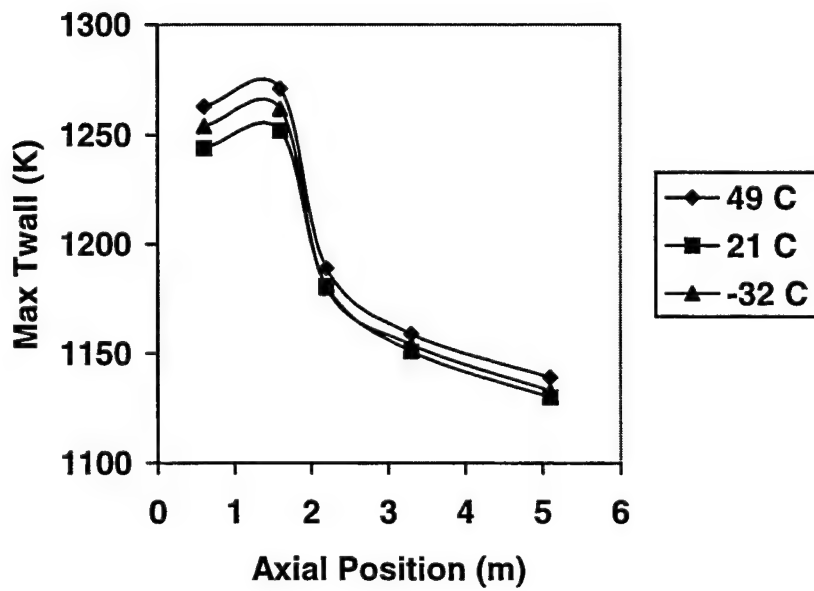


Figure 10. M829E3 MACE A723 interface temperature.

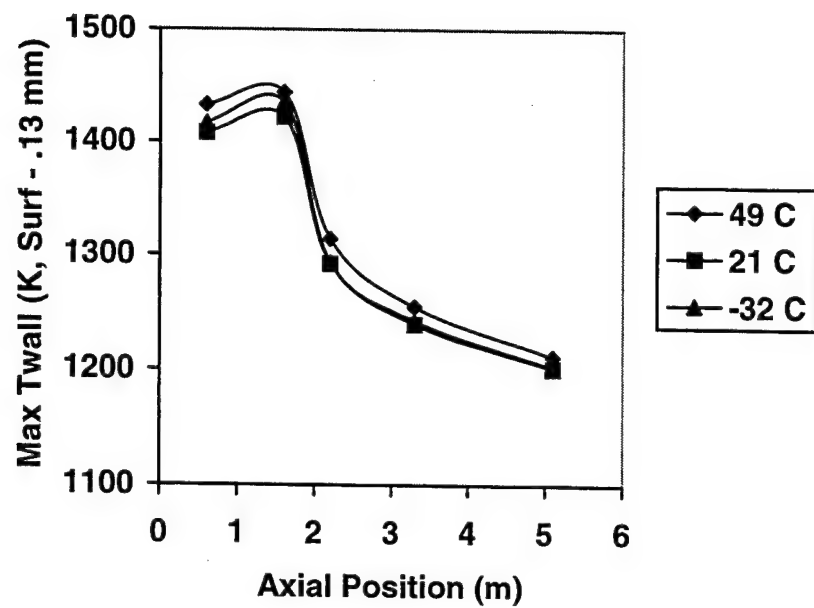


Figure 11. M829E3 MACE A723 surface temperature.

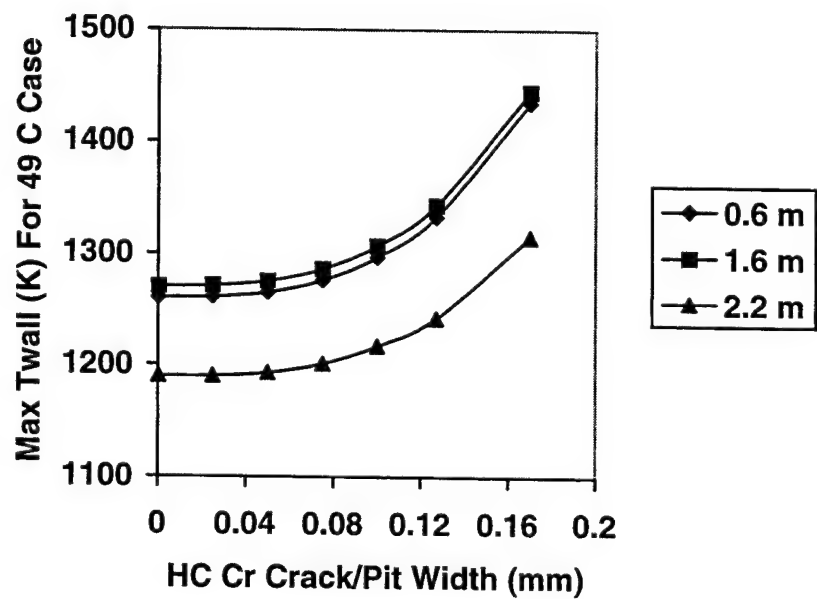


Figure 12. M829E3 exposed interface temperature.

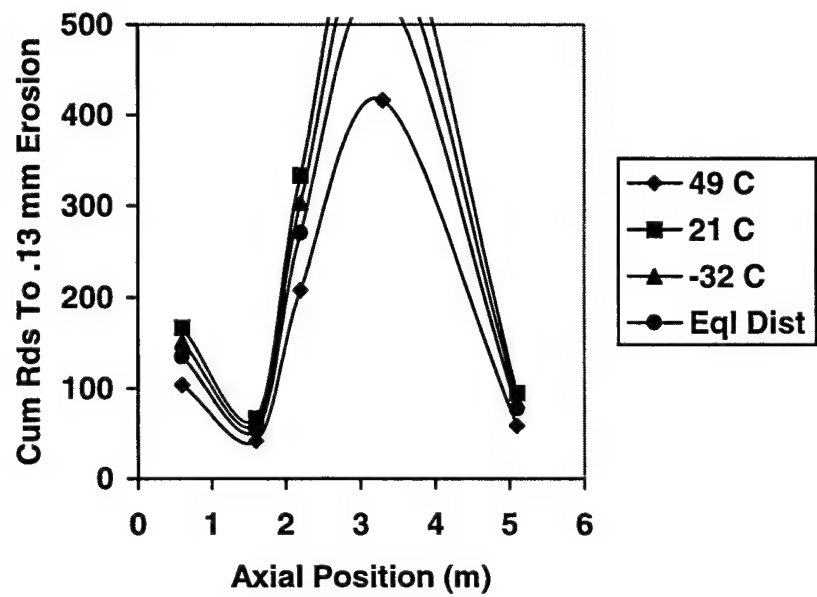


Figure 13. M829E3 erosion onset.

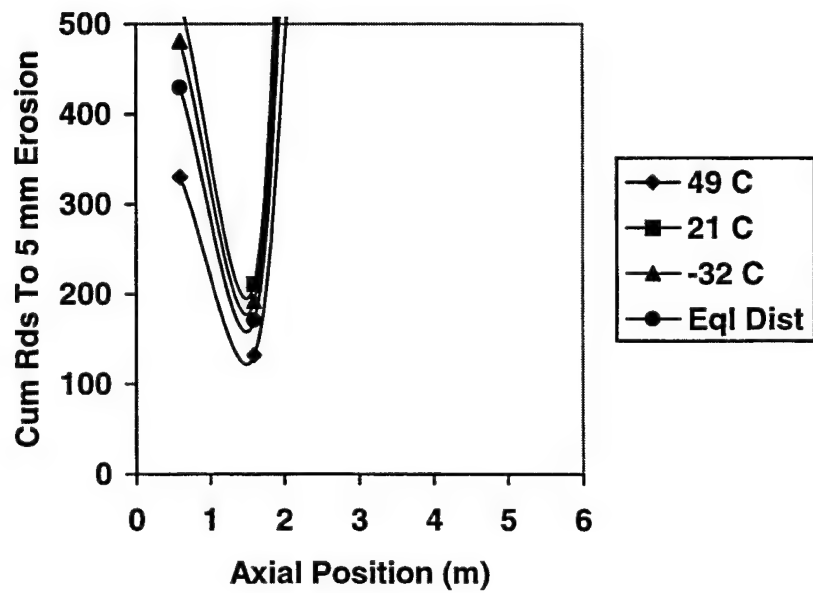


Figure 14. M829E3 erosion condemnation.

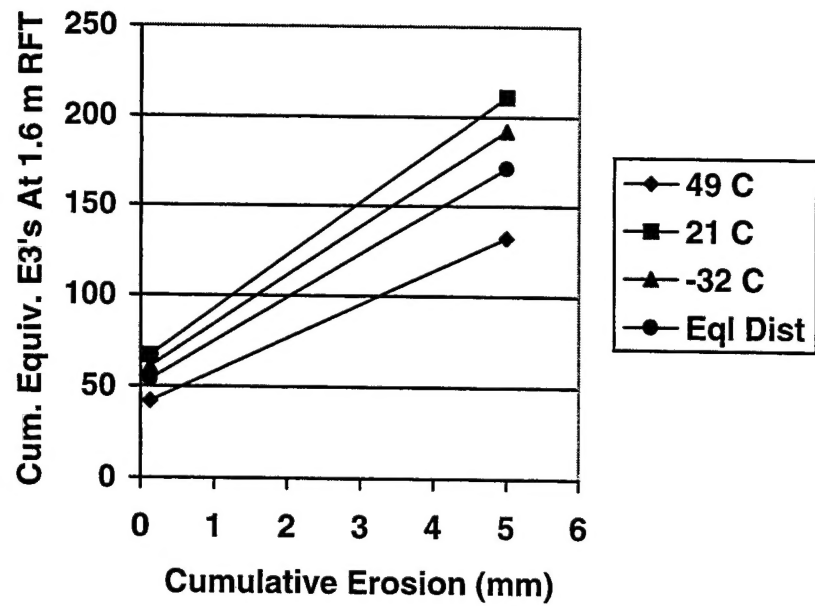


Figure 15. M829E3 erosion summary.

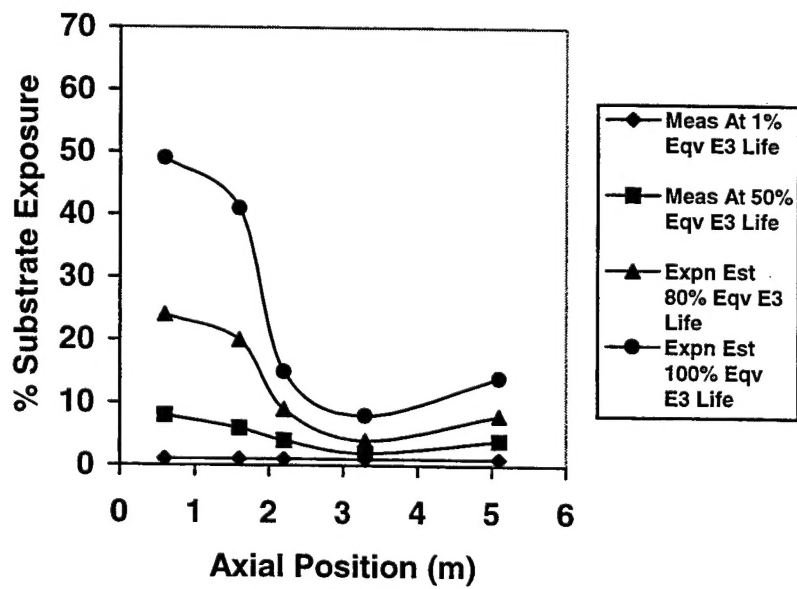


Figure 16. E3/HEAT M256 substrate exposure.

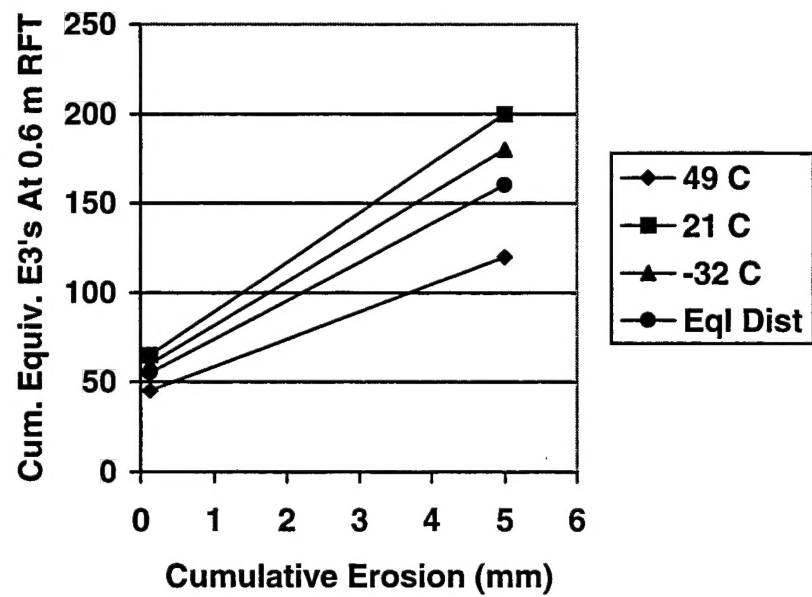


Figure 17. M829E3/HEAT erosion summary.

TECHNICAL REPORT INTERNAL DISTRIBUTION LIST

	<u>NO. OF COPIES</u>
TECHNICAL LIBRARY ATTN: AMSTA-AR-CCB-O	5
TECHNICAL PUBLICATIONS & EDITING SECTION ATTN: AMSTA-AR-CCB-O	3
OPERATIONS DIRECTORATE ATTN: SIOWV-ODP-P	1
DIRECTOR, PROCUREMENT & CONTRACTING DIRECTORATE ATTN: SIOWV-PP	1
DIRECTOR, PRODUCT ASSURANCE & TEST DIRECTORATE ATTN: SIOWV-QA	1

NOTE: PLEASE NOTIFY DIRECTOR, BENÉT LABORATORIES, ATTN: AMSTA-AR-CCB-O OF ADDRESS CHANGES.

TECHNICAL REPORT EXTERNAL DISTRIBUTION LIST

	<u>NO. OF COPIES</u>		<u>NO. OF COPIES</u>
DEFENSE TECHNICAL INFO CENTER		COMMANDER	
ATTN: DTIC-OCA (ACQUISITIONS)	2	ROCK ISLAND ARSENAL	
8725 JOHN J. KINGMAN ROAD		ATTN: SIORI-SEM-L	1
STE 0944		ROCK ISLAND, IL 61299-5001	
FT. BELVOIR, VA 22060-6218			
COMMANDER		COMMANDER	
U.S. ARMY ARDEC		U.S. ARMY TANK-AUTMV R&D COMMAND	
ATTN: AMSTA-AR-WEE, BLDG. 3022	1	ATTN: AMSTA-DDL (TECH LIBRARY)	1
AMSTA-AR-AET-O, BLDG. 183	1	WARREN, MI 48397-5000	
AMSTA-AR-FSA, BLDG. 61	1	COMMANDER	
AMSTA-AR-FSX	1	U.S. MILITARY ACADEMY	
AMSTA-AR-FSA-M, BLDG. 61 SO	1	ATTN: DEPT OF CIVIL & MECH ENGR	1
AMSTA-AR-WEL-TL, BLDG. 59	2	WEST POINT, NY 10966-1792	
PICATINNY ARSENAL, NJ 07806-5000			
DIRECTOR		U.S. ARMY AVIATION AND MISSILE COM	
U.S. ARMY RESEARCH LABORATORY		REDSTONE SCIENTIFIC INFO CENTER	2
ATTN: AMSRL-DD-T, BLDG. 305	1	ATTN: AMSAM-RD-OB-R (DOCUMENTS)	
ABERDEEN PROVING GROUND, MD		REDSTONE ARSENAL, AL 35898-5000	
21005-5066			
DIRECTOR		COMMANDER	
U.S. ARMY RESEARCH LABORATORY		U.S. ARMY FOREIGN SCI & TECH CENTER	
ATTN: AMSRL-WM-MB (DR. B. BURNS)	1	ATTN: DRXST-SD	1
ABERDEEN PROVING GROUND, MD		220 7TH STREET, N.E.	
21005-5066		CHARLOTTESVILLE, VA 22901	
COMMANDER			
U.S. ARMY RESEARCH OFFICE			
ATTN: TECHNICAL LIBRARIAN	1		
P.O. BOX 12211			
4300 S. MIAMI BOULEVARD			
RESEARCH TRIANGLE PARK, NC 27709-2211			

NOTE: PLEASE NOTIFY COMMANDER, ARMAMENT RESEARCH, DEVELOPMENT, AND ENGINEERING CENTER,
 BENÉT LABORATORIES, CCAC, U.S. ARMY TANK-AUTOMOTIVE AND ARMAMENTS COMMAND,
 AMSTA-AR-CCB-O, WATERVLIET, NY 12189-4050 OF ADDRESS CHANGES.
